

# Fine structure, hyperfine structure, and Stark effect in the NO $A^2\Sigma^+$ state by optical radio-frequency double resonance

T. Bergeman

Columbia Radiation Laboratory, Columbia University, New York, New York 10027 and  
Department of Physics\*, Fordham University, Bronx, New York 10458

R. N. Zare

Columbia Radiation Laboratory and Department of Chemistry, Columbia University, New York, New York 10027

(Received 15 May 1974)

Using the Se I 1961 Å spectral line to pump the  $J = 3/2$  component of the  $\nu = 3, N = 1$  level of the NO  $A^2\Sigma^+$  state, we observe the zero-field rho-doubling hyperfine transitions by optical radio-frequency double resonance. The Stark shift of one of the resonance components is measured to determine the permanent electric dipole moment. An analysis of the resonance line shapes yields the following molecular constants: The rho-doubling constant  $\gamma = -82.91 \pm 0.03$  MHz; the hyperfine parameters of the  $^{14}\text{N}$  nucleus  $b = 40.29 \pm 0.07$  MHz,  $c = 2.25 \pm 0.11$  MHz, and  $eqQ = -2.88 \pm 0.17$  MHz; and the dipole moment  $\mu = 1.10 \pm 0.03$  D, where all errors represent three standard deviations. The value of  $\gamma$  is explained reasonably well by calculations of the  $A-X$  spin-orbit mixing from which we conclude that variations of  $\gamma$  with  $\nu$  and  $N$  are small. The values of the hyperfine parameters  $b$  and  $c$  are within 6% and 18% of recent CI calculations by S. Green, while the less well determined values of  $eqQ$  differ by about a factor of 2. The measured dipole moment differs considerably from the CI value,  $\mu = 0.40 \pm 0.10$  D. We speculate on possible explanations for this surprisingly large discrepancy.

## INTRODUCTION

Molecular Rydberg states have been a source of fascination for many years. The general characteristics of Rydberg orbitals and the variety of couplings with the ion core as a function of  $l$  and (for diatomic molecules)  $\Lambda$  have been discussed in broad outline by Mulliken.<sup>1</sup> More precise theoretical calculations have been performed for particular molecular Rydberg states recently.<sup>2</sup> Interest in such states has also been stimulated by the role they play in ionization, recombination, dissociation, and other rearrangement processes. With the development of techniques for high resolution spectroscopic studies in the vacuum ultraviolet region of the spectrum, the excited states of the NO molecule have been extensively studied. Because the first ionization limit of NO, at  $74770\text{ cm}^{-1}$ , falls within the spectral range of these techniques and because the  $\text{NO}^+$  core is a stable closed shell, the Rydberg states of NO are as well known as those of any diatomic molecule. Thanks to the careful work of Miescher and collaborators,<sup>3</sup> numerous sequences of excited states have been identified in which the outer electron assumes hydrogen-like  $n\Lambda$  orbitals ( $n \geq 3$ ) centered about the  $\text{NO}^+$  core. After certain perturbation interactions are considered, these sequences are found to follow very closely the Rydberg formula

$$\nu_n = \nu_\infty - \frac{R}{(n - \delta_{l\Lambda})^2}, \quad (1)$$

where  $\nu_\infty$  is the first ionization limit,  $R$  is the Rydberg constant, and  $\delta_{l\Lambda}$  is the quantum defect for the  $l\Lambda$  sequence. While Eq. (1) has been shown to apply reasonably well for the electronic energies, many questions about other properties of Rydberg states remain unan-

swered. We undertook this study to obtain a set of experimental parameters that could be compared with *ab initio* calculations for a molecular Rydberg state.

Previously, fine and hyperfine structure measurements of molecular Rydberg states by Doppler-free techniques have been limited to a few states of  $\text{H}_2$  and  $\text{D}_2$ .<sup>4</sup> Using a variation of the optical-radio-frequency double resonance technique (ODR),<sup>5</sup> we have measured the fine structure, hyperfine structure, and Stark effect in the NO  $A^2\Sigma^+$  state. This is the lowest-lying NO Rydberg state and is conventionally described by a  $3s\sigma$  electron outside the  $\text{NO}^+$  ion core. However, the interpretation of the measured properties suggests certain departures from this rudimentary description.

The fine structure of the  $A$  state consists of the rho-doubling, which splits each rotational level  $N$  into two components,  $J = N \pm \frac{1}{2}$ . The rho-doubling parameter,  $\gamma$ , in the case of the NO  $A$  state has heretofore eluded the most careful analyses of the optical spectra<sup>6</sup>; our ODR value, however, is reported to  $\pm 0.04\%$ . It appears that for this loosely bound electron, as for most other  $^2\Sigma^+$  states, off-diagonal elements of the spin-orbit operators are primarily responsible for  $\gamma$ . With the help of *ab initio* calculations, we conclude that  $A-X$  spin-orbit mixing provides the predominant contribution to  $\gamma$ .

The hyperfine structure of the NO  $A$  state is characterized by three interactions; Fermi contact, electron-spin-nuclear-spin dipole-dipole, and nuclear quadrupole coupling. In these experiments, the spin density at the  $^{14}\text{N}$  nucleus dominates the hyperfine structure. The value of the Fermi contact term furnishes a stringent test of configuration interaction calculations. Unlike the situation in alkali atoms or in  $\text{H}_2$ , the lowest excitation energies for electrons excited from the ion core are comparable to Rydberg excitation energies for NO. Thus

Rydberg–non-Rydberg configuration interaction plays a more important role in NO than in H<sub>2</sub>. The experimentally determined Fermi contact term differs significantly from single configuration SCF calculations, but agrees quite well with the CI wavefunction result.

The shift of  $|F, m\rangle$  levels in an electric field is characterized by a permanent electric dipole moment  $\mu$ , after a small polarizability correction is made. The Stark effect reported here is the first determination of a dipole moment for a molecular Rydberg state. The observed dipole moment differs from a convergent CI calculation for fixed nuclei performed at  $R=r_e$  by more than a factor of 2. We suggest that the mixing of the  $D^2\Sigma^*(3p\sigma)$  Rydberg state, lying one electron volt higher, either through configuration interaction at  $R > r_e$  or through nonadiabatic effects, may be responsible for part of the apparent excited state dipole moment.<sup>7,8</sup> Presently, we have no confirmation of these possibilities. Consequently, there is a need for additional experiments beyond those that were possible here in order to supply additional confirmation of the experimental value, to obtain, for example, the vibrational dependence of  $\mu$ , and to shed light on the discrepancy with existing calculations.

The data we present are made possible by resort to relatively new experimental techniques. Recent work on the NO A–X band system has reached what is probably the limit of accuracy of optical absorption spectroscopy. The line positions of Engleman *et al.*,<sup>6d</sup> which we use in the interpretation of our ODR data, are limited by the Doppler effect to an accuracy of about 0.01 cm<sup>-1</sup> (300 MHz). A number of techniques have been developed recently which are limited by radiative linewidth, rather than the Doppler width. Laser saturation spectroscopy, level crossing, and optical double resonance have all been successfully applied to excited states of molecules.<sup>9</sup> However, there are difficulties in applying the previous methods to the NO A state. For example, at present there are no lasers of the desired pumping frequency; the intermediate-field Zeeman effect consists of dense, overlapping lines; and high-field magnetic resonance suffers from poor state selection and hence low resonance intensities.

The technique we have selected utilizes, as in several previous experiments on molecular excited states, optical pumping by an intense atomic spectral line. The 1961 Å Se I line happens to coincide with the  ${}^oP_{12}(\frac{5}{2})$  absorption line in the (3, 0) A–X band, thereby selecting the  $J = \frac{3}{2}$ ,  $N = 1$ ,  $v = 3$  level of the A state.<sup>10</sup> To simplify the spectrum and enhance the rf resonance intensities, the hyperfine spectrum is observed by monitoring the fluorescence at zero field, a procedure that has been applied elsewhere with Rb atoms.<sup>11</sup> For the Stark effect measurements, a static electric field is applied across the scattering region, within the rf loop. Theoretical intensities and resonance line shapes for the zero-field transitions, including off-resonant interference effects, are discussed in detail in an accompanying paper<sup>12</sup> (hereafter referred to as II). By applying this theory to signal-averaged ODR data, resonance line centers are measured to an accuracy of 50–200 kHz, which is a

small fraction of the 2 MHz radiative linewidth.

## I. ZERO-FIELD SPECTRUM

### A. The energy level structure and rf spectrum of the NO A ${}^2\Sigma^+$ state

The A state of NO, like the majority of  ${}^2\Sigma^+$  states, is well described by case  $b_{b,J}$  coupling<sup>13</sup> for which the rotational spacings are large compared to the fine-structure splittings caused by electron-spin–nuclear-rotation coupling, which in turn is large compared to the hfs splittings caused by electron-spin–nuclear-spin coupling. Of course, in actually computing matrix elements of the molecular Hamiltonian, it is often more convenient to use a Hund's case (a) basis set for which  $S_z$ , the component of the electron spin  $S$  along the internuclear axis, makes the projection  $\Sigma$ .

The molecular Hamiltonian consists of electronic, vibrational, and rotational terms, plus the following fine and hyperfine structure elements for a molecule in which one nucleus has nonzero spin<sup>14</sup>:

$$H = \gamma(N \cdot S) + b(I \cdot S) + cI_z S_z + eQq[3I_z^2 - I(I+1)]/4I(2I-1). \quad (2)$$

Here,  $\gamma$  is the rho-doubling constant,

$$b = g_I \mu_0 \mu_N [16\pi/3\Psi^2(0) - 2\langle P_2(\cos\chi)/r^3 \rangle_{av}], \quad (3)$$

$$c = 6g_I \mu_0 \mu_N \langle P_2(\cos\chi)/r^3 \rangle_{av}, \quad (4)$$

and

$$q = 2 \sum_i e_i \langle P_2(\cos\chi_i)/r_i^3 \rangle_{av}, \quad (5)$$

where the argument of the Legendre polynomial  $P_2(z) = (3z^2 - 1)/2$  is the cosine of the angle  $\chi$  measured from the internuclear axis to the coordinate of the electron,  $r$  is the distance between the electron and the nucleus with spin  $I$ ,  $\Psi^2(0)$  is the probability density of unpaired electrons at this nucleus,  $\mu_N$  is the nuclear Bohr magneton,  $g_I$  the nuclear  $g$  factor,  $\mu_0$  the electronic Bohr magneton, and  $N$  is the nuclear rotation operator. The integrals in  $b$  and  $c$  are taken over the unpaired electron or electrons, while for  $q$  the sum runs over all electrons and the magnetically nonactive nucleus. The term in  $\gamma$ , which has the form of an electron-spin–nuclear-rotation interaction, has been shown in almost all  ${}^2\Sigma$  states previously examined to arise from off-diagonal spin–orbit interactions with  ${}^2\Pi$  states.<sup>15</sup> In Sec. IV, we show that this interpretation may also be applied to the A state of NO.

Matrix elements of the hyperfine terms are evaluated by Frosch and Foley<sup>14a</sup> in general and by Radford<sup>14b</sup> for  ${}^2\Sigma$  states. German *et al.*<sup>16</sup> give specialized formulas for  $N=1$  levels of  ${}^2\Sigma$  states having one magnetically active nucleus with  $I=1$ , such as applies to  ${}^{14}\text{N}$   ${}^{16}\text{O}$ . Figure 1 depicts the energy level scheme derived from the results of the present study.

A first-order calculation of rf transition intensities for the double resonance technique was used to select the optimum experimental configuration and to assign the observed resonances. A more exact theory that does

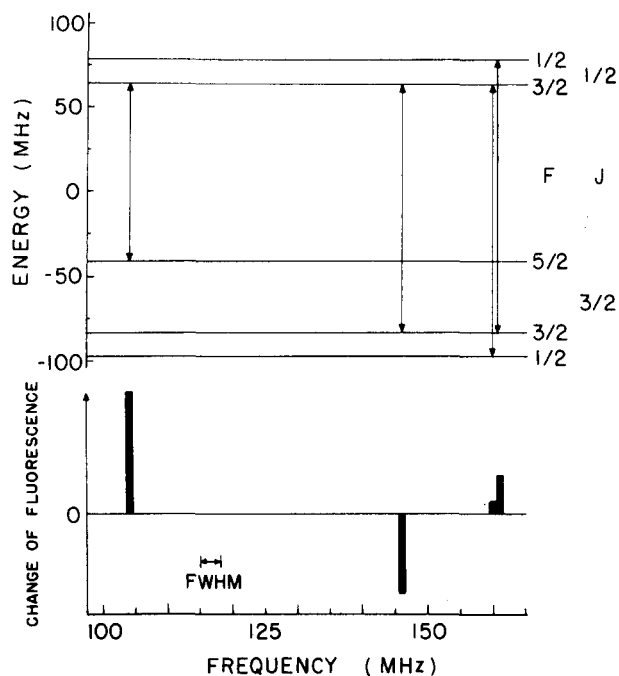


FIG. 1. Energy level diagram and theoretical ODR intensities for zero-field transitions with 1 G rf magnetic field in  $v=3$ ,  $N=1$  of the NO A  $2\Sigma^+$  state. The relative (but not absolute) intensities are nearly independent of experimental geometry.

not assume Lorentzian line shapes for the rf resonances is presented in Paper II. This improved formulation was used to extract line centers from the final data.

Because NO has an odd electron, the most convenient rf transition is the magnetic dipole, "electron-spin flip" across the doublets  $J=N+\frac{1}{2}$  and  $J=N-\frac{1}{2}$ . The observed intensity depends on the ability of this magnetic dipole transition to reorient the electric dipole optical transition moment. Intensities may be calculated from the transition elements  $\langle i | \mu \cdot \mathbf{B}_{rf} | j \rangle$  (where  $\mu$  is the magnetic moment operator of the molecule and  $\mathbf{B}_{rf}$  is the rf magnetic field), the radiative lifetime, and from the density matrices for the excitation and fluorescence processes (See Table III of Paper II). For  $N=1$  and  $I=1$ , matrix elements for the rho-doublet transitions in a  $2\Sigma^+$  state vary from  $0.3 \mu_0$  to  $0.8 \mu_0$  depending upon the strength of the hyperfine coupling. If one neglects off-resonance effects, which contribute less than 10% of the signal, the relative intensity of the zero-field resonance may be calculated from Eq. (17) of Paper II. Figure 1 (lower portion) shows typical results for the relative intensity of the double resonance signals when the rotational branches of the molecular fluorescence are not resolved.

To select the best geometry, such calculations were performed for various orthogonal orientations of the propagation and polarization vectors of excitation and fluorescence, and of  $\mathbf{B}_{rf}$ . As shown in Paper II, the experimental arrangement that gives the best signal: noise ratio is with the exciting light unpolarized and the fluorescence analyzed for the component polarized along the direction of the rf field. Sufficient state selection is produced with this configuration because the  ${}^{\circ}P_{12}(\frac{5}{2})$  transition pumped by the 1961 Å Se I line<sup>10</sup> populated only the

$J=\frac{3}{2}$  level of the upper state.

The transition intensities in Fig. 1 were computed with the final values of the molecular parameters obtained in this study. Qualitatively similar results are expected for any  $2\Sigma$  molecule following case  $b_{\beta J}$  coupling. Therefore, conclusions obtained from calculations based on preliminary estimates of the molecular parameters were valid once it was established that this coupling scheme did apply.

## B. Experimental

The technique employed in this study utilizes a selenium lamp optical pumping source; a scattering cell, including Stark plates when desired; an rf oscillator to provide a constant rf field of  $\sim 1$  G over a 10–30 MHz scan; photodetector; and signal averaging equipment.

The atomic lamp was an electrodeless discharge tube containing selenium vapor with 0.5 torr argon buffer gas. A 120 W 2450 MHz magnetron was the power supply. Because of the relatively high vapor pressure of selenium (1 torr at 350 °C), the lamp output tended to be rather unstable except with a carefully regulated cooling air stream and long equilibration. At best, there were 5% output variations over an hour. Under optimum conditions, the 1961 Å line, with other members of the  $4p^3 5s^3 S - 4p^4 3P$  triplet, constituted the only spectral features observed with a scanning monochromator over the range of maximum sensitivity of the phototube. Therefore, even without bandpass filtering of the exciting light or of the fluorescence, the instrumentally scattered light was only 10%–20% of the fluorescent light despite the relatively weak  ${}^{\circ}P_{12}(\frac{5}{2})$  (3, 0) pumping transition.

For the zero-field experiments, the nitric oxide was contained in a 1 in. diam pyrex tube with a Wood's horn that was abruptly tapered so as not to extend into the region of higher rf electric field (see below). Quartz windows were epoxied to front and side apertures. The NO was maintained approximately at average pressures of 25–150 mtorr, measured by a Pirani gauge with air calibration. Because of photodissociation losses, however, there was a 15%–33% decay of the NO density per hour. Although the bulb was refilled periodically during long signal averaging, accurate pressure dependence of the linewidths could not be obtained with this arrangement, and is not reported here.

Because of the excellent state selection of the  $J=\frac{3}{2}$ ,  $N=1$  hfs components via the  ${}^{\circ}P_{12}(\frac{5}{2})$  transition, no polarizer was needed on the pumping light. For the fluorescence, which was most intense in the (3, 1) and (3, 4) bands at 2050 Å and 2450 Å, respectively, a selected Polacoat UV-105 polarizing filter, with relatively high transmission (50% of the preferred component) and moderate efficiency (90%) was used. This resulted in a theoretical advantage of 2:1 in signal: noise ratio over the detection of unpolarized fluorescence. The optical train also contained quartz lenses and an RCA 1P28 phototube. Observed photocurrents corresponded to about  $10^8$  photoelectrons/sec.

The vital part of the apparatus, however, was the rf oscillator. Several novel features were incorporated in

a conventional vacuum tube device so as to meet the requirements of zero-field resonance experiments. The usual variable-frequency oscillator, tuned-amplifier, tuned-load arrangement would have required a complicated ganged tuning mechanism. It was simpler to place the scattering cell in the loop inductor of a single-stage oscillator. In this case, the rf field is quite constant with frequency without adjustment of the input power. A schematic of such a unit is shown in Fig. 2.

For these experiments, the resonant tank circuit consisted of a copper strap loop inductor and a plunger capacitor with a quartz dielectric (Johanson, JMC 7034) mounted directly on the plate leads of a 5894 dual tetrode.<sup>17</sup> For the 130–180 MHz range, the strap was 5 in. long,  $1\frac{1}{2}$  in. wide, with a 1 in. radius of curvature at the cell end. The capacitor variation of 0–10 pF sufficed for this range, while lower frequencies were obtained by adding low-impedance, high- $Q$  fixed capacitors (JFD Electronics Co., UFP) or by lengthening the strap. The use of a broad strap was intended to remove high edge fields away from the cell and to help make the magnetic field as uniform as possible over the scattering region. Modifications of this design spanning the range 20–250 MHz were used in the initial resonance searches.

A 1 G rf magnetic field, directed vertically in Fig. 2, was produced with about 12 W input power. Although much of this power is dissipated in the tube itself, in view of a 40 W plate dissipation rating and ample blower cooling, frequency drifts due to thermal effects were less than 1 kHz/h. Because of the simplicity of the circuit, parasitic resonances, observed as waveform distortions on a sampling oscilloscope, could be essentially eliminated by proper adjustment of the feedback capacitors. A wire loop probe inserted into the resonance region indicated that over a 20 MHz scan, the amplitude of the rf field is constant to at least the 3% measurement precision of the sampling oscilloscope used as a detector.

Whereas a solenoidal coil produced gaseous discharge

in the scattering cell at quite low power levels, the copper strap, which resembles a shorted transmission line, allows for a minimum ratio of rf electric field (which produces discharge) to rf magnetic field. If  $z$  is the distance from the shorted end, the amplitude of the rf electric field,  $E_{rf}$ , varies as  $H_1 \cos kz$ .<sup>18</sup> For frequencies of interest,  $1/k = \lambda/2\pi$  is  $> 30$  cm. Consequently, a cell of 3 cm length placed at the shorted end is exposed to essentially the peak  $H_{rf}$  amplitude, but less than one-tenth the peak value of  $E_{rf}$ . From the geometry, it may be estimated that 10–15 A peak rf current in the loop produces 1 G  $H_{rf} = H_1$  at the cell. For a characteristic impedance of about 250  $\Omega$ , one has  $E_1 = 600$  V/cm across the 5 cm strap. Over the cell itself,  $kz$  is less than 0.1, so that for  $H_{rf}$  equal to 1 G,  $E_{rf}$  is less than 60 V/cm (estimated to within a factor of 2). While this level of rf electric field was tolerable, an increase of 50% by raising the plate input power or the frequency generally led to gaseous discharge breakdown of the NO gas in the scattering cell.

A rough measure of the rf magnetic field strength by Faraday induction gave a value about 20% larger than that obtained from fitting the spectra (see Sec. III). The fitted values were consistent to 3% between runs and are undoubtedly more reliable because of effects of stray capacitance and inductance on the probe leads that were inserted into the loop.

The scan over frequency was accomplished by coupling the plunger capacitor to a micrometer screw driven by a stepping motor. The motor in turn was activated by programmed pulses from a PDP-8S computer that handled the signal averaging tasks. Each step ( $1.8^\circ$ ) of the motor advanced the plunger  $2.5 \mu$ , and shifted the frequency 10 kHz in the 130–180 MHz range, or 3 kHz near 100 MHz. Typically, 35 channels were used per 10 MHz. To reduce the effect of lamp fluctuations, the screen voltage ( $E_s^+$  in Fig. 2) was modulated at 13 Hz, and the photocurrent was amplified by a phase-sensitive detector whose output was digitized for purposes of signal averaging. All final data points, such as those

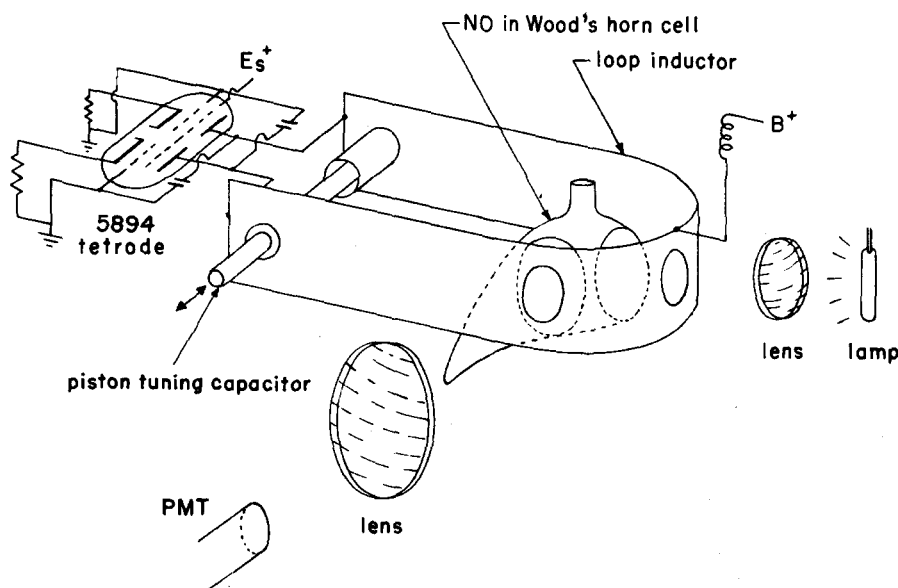


FIG. 2. Schematic diagram showing the nitric oxide scattering cell placed in the tank circuit of an rf oscillator whose frequency is scanned by varying a piston tuning capacitor.

shown in Figs. 3 and 4, were obtained by averaging up and down frequency scans. At the start and end of each data run, the frequency was recorded at the end points of each channel using a subroutine that advanced the scan one channel at a time, on command. A Monsanto 105 A counter was used. Mechanical hysteresis, or backlash, in the scanning device was no more than 30 kHz, so that each averaged channel midpoint frequency is accurate to 15 kHz or better. Because of the limitation of the signal: noise ratio, and the large linewidth, it was not deemed profitable to perfect the mechanism beyond this level.

### C. Data, analysis, and results

Data obtained for zero-field resonances with the above procedure are presented in Figs. 3 and 4. The data for Fig. 3 were obtained by 2 h signal averaging, with 50 mtorr NO pressure and about 0.7 G rms rf field. Figure 4, which shows the blended lines near 160 MHz, is the result of 6 h averaging with 35 mtorr NO, and about 1.1 G rms rf field.

While line centers of the 104 and 146 MHz lines may be deduced fairly well by graphical methods, the blended lines at 160 MHz require more careful treatment. When scans for the region 150–165 MHz are fit to Lorentzian profiles associated with each transition, it is found that the fitted intensities and widths do not correspond to predictions from theoretical population differences and transition moments. Conversely, when the state selections and transition elements are fixed at calculated values, the least squares fit, shown by the dashed line in Fig. 5, exhibits a clear discrepancy with the data. The fit actually requires a  $\Gamma = (2\pi\tau)^{-1}$  which is too small compared with the other lines and with other lifetime data on the NO  $A$  state, and predicts an inflection between the blended lines, as shown, which is not observed. Neither this nor the discrepancies in the wings can be explained by plausible variations of the field with frequency, rf

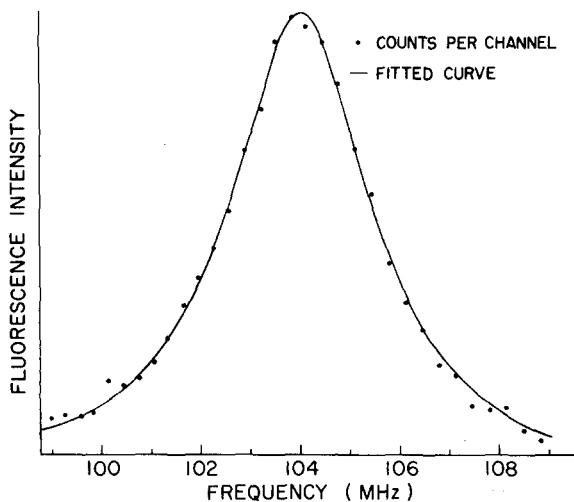


FIG. 3. Resonance line shape obtained for the  $F = \frac{5}{2}, J = \frac{3}{2} \leftrightarrow F = \frac{3}{2}, J = \frac{1}{2}$  transition. The solid line represents the best fit to the five-level interaction theory (see paper II), which includes rf interference effects that produce a slight asymmetry.

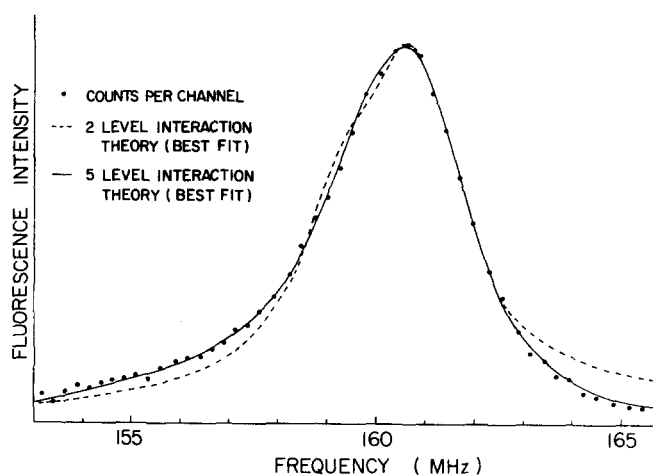


FIG. 4. Resonance line shape for the blended pair of transitions shown in Fig. 1. The fit to the two-level interaction theory (dashed line) uses pure Lorentzian line shapes of a known intensity ratio, while the fit to the five-level interaction theory (solid line) introduces rf interference effects.

power broadening, or by spurious perpendicular components of the rf field. The fact that these discrepancies occurred consistently in repeated scans led to the formulation of more complete resonance equations, which are developed in Paper II.

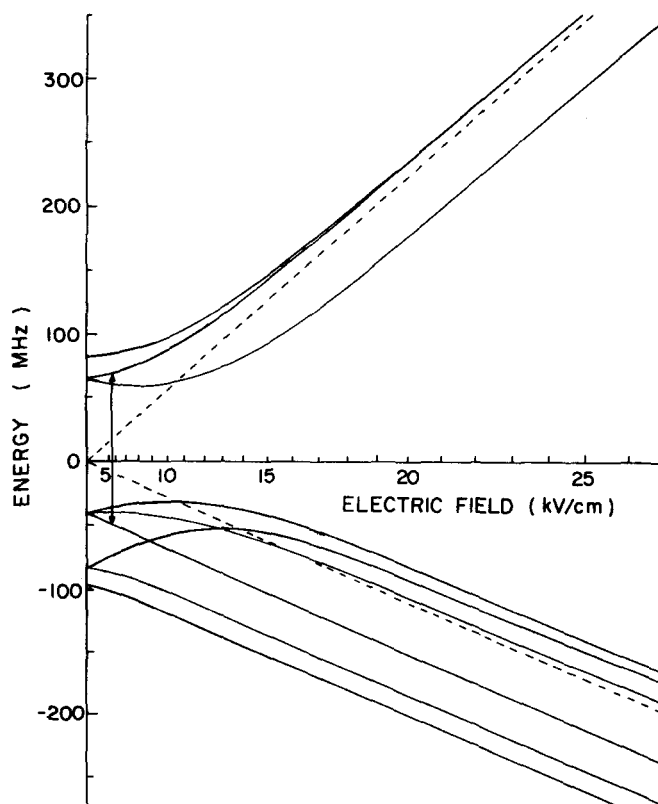


FIG. 5. Energy level pattern plotted against the square of the electric field for the  $N=1, v=3$  hyperfine components of NO  $A^2\Sigma^+$ . The arrow represents the rf transition observed in this work. The dashed lines represent the behavior of  $J=N=1$  levels of a  $^1\Sigma^+$  state having the same dipole moment with no hyperfine structure.

Briefly, what is involved is interference between different near-resonant rf transitions. These effects are expressed formally as contributions from elements of the density matrix off-diagonal in  $F$ , induced by the rf field. Since these effects depend on frequency, there will be a distortion of the line shape from pure Lorentz character. To calculate this effect, the full interaction Hamiltonian for each  $m$  manifold (five states for  $|m| = \frac{1}{2}$ , three for  $|m| = \frac{3}{2}$ ) is used, rather than considering each pair of resonant states separately. The final analysis was performed with a least squares fitting program based on this approach. The much-improved quality of the fit is demonstrated by the solid line in Fig. 4. This more complete analysis results in a value for the  $F = \frac{1}{2} - \frac{3}{2}$ ,  $J = \frac{3}{2} - \frac{1}{2}$  transition which differs by 2 MHz from that obtained from Lorentzian line fits, while the value for the more intense  $F = \frac{3}{2} - \frac{1}{2}$ ,  $J = \frac{3}{2} - \frac{1}{2}$  line differs by 0.4 MHz. Since these differences are 8–10 times the experimental errors and are comparable in magnitude to the two smaller hyperfine parameters, the relevance of the improved analysis is clearly demonstrated. Also, the complete theory of the interference effects leads to corrections of 0.08 and 0.1 MHz, respectively, to the apparent centers of the 104 and 146 MHz lines. On the other hand, Bloch–Seigart corrections from the “counter-rotating” component and from rf interactions diagonal in  $J$  were less than 15 kHz, as discussed in Paper II.

This type of analysis depends on an approximate determination of the experimental parameter  $B_{rf}$ . For a “standard setting” of oscillator input voltages, direct measurement by Faraday induction with the small loop probe gave 1.25 G (rms), while least squares fit to spectral scans over the 135–165 MHz region gave 1.06 G. As mentioned previously, the first method is sensitive to stray inductance and capacitance in the probe circuit. The latter method is based on the relative power dependence of the intensities and widths of the 146 and 160–161 MHz lines and is sensitive to variations of the field, perhaps even within the 3% limit of detectable variations. A weighted average of  $1.1 \pm 0.2$  G was used in analyzing several runs, such as depicted in Fig. 4, over the 153–164 MHz region at the “standard” power level. This uncertainty in the field introduces uncertainties of only 0.08 and 0.03 MHz into the extraction of the line centers for the 160 and 161 MHz lines, respectively, which increases their total uncertainties by about 25%. Table I gives the final determinations of the line

TABLE I. Zero-field resonance frequencies in  $v=3$ ,  $N=1$ , NO A  $2\Sigma^+$ . The uncertainties represent three standard deviations.

$F_1$	$J_1$	$F_2$	$J_2$	Frequency (MHz)
$\frac{5}{2}$	$\frac{3}{2}$	$\frac{3}{2}$	$\frac{1}{2}$	$104.053 \pm 0.06$
$\frac{3}{2}$	$\frac{3}{2}$	$\frac{3}{2}$	$\frac{1}{2}$	$146.128 \pm 0.03$
$\frac{1}{2}$	$\frac{3}{2}$	$\frac{3}{2}$	$\frac{1}{2}$	$159.674 \pm 0.15$
$\frac{3}{2}$	$\frac{3}{2}$	$\frac{1}{2}$	$\frac{1}{2}$	$160.914 \pm 0.1$

TABLE II. Structural parameters for the NO A  $2\Sigma^+$  state, as measured in  $v=3$ ,  $N=1$ . Calculated values from Green are presented for comparison. The uncertainties represent three standard deviations.

Parameter	Value	SCF <sup>a</sup>	CI <sup>b</sup>
$b$	$40.29 \pm 0.07$ MHz	27.27 MHz	38.06 MHz
$c$	$2.25 \pm 0.11$	1.36	2.63
$eqQ$	$-2.88 \pm 0.17$	-6.64	-5.62
$\gamma$	$-82.91 \pm 0.03$		
$\mu$	$1.10 \pm 0.03$ D	0.62 D	0.39 D

<sup>a</sup>Reference 32.

<sup>b</sup>Reference 31.

positions with  $3\sigma$  uncertainties.

To obtain molecular parameters, the zero-field resonance frequencies obtained from the line shape fits were fit to the Hamiltonian by optimizing  $\gamma$ ,  $b$ ,  $c$ , and  $eqQ$ . Table II gives the results, with 3 times the standard deviations produced by the fitting program.<sup>19</sup> The quoted uncertainties of the parameters vary because all resonances combine to determine the rho-doubling constant, while differences in the measured frequencies determine the hyperfine constants: in particular, the differences with the most poorly determined line, at 160 MHz, determine  $c$  and  $eqQ$ .

An approximate value for the radiative lifetime of the upper state may be obtained from the line shape fits. From four scans performed at 25 mtorr NO, an average effective lifetime  $\tau = 135 \pm 25$  nsec is obtained. Because of the photodissociative decay of NO, the pressure effect has not been obtained, as indicated above. A rough estimate of the pressure dependence may be obtained from the Hanle effect data for  $v=1$ ; from the most recent study,<sup>20</sup> the correction at 25 mtorr is 9%, which can be considered accurate to no more than a factor of 2 when applied to rf transitions in  $v=3$ . Consequently, the estimate for the radiative lifetime is  $\tau = 150 \pm 40$  nsec. This value is not accurate enough to verify the suggestion from emission band intensities that the transition moment rapidly decreases beyond  $r$ -centroid values of  $1.1 \text{ \AA}$ .<sup>21</sup> It is a reasonable extrapolation from the  $v=1$  lifetime values of  $180 \pm 20$  nsec from the Hanle effect,<sup>20</sup> and is also approximately consistent with the Hook method oscillator strength measurements.<sup>22</sup>

## II. STARK EFFECT

### A. Hamiltonian matrix elements and computed Stark spectrum

Because the Stark effect of a  $2\Sigma^+$  state with hyperfine structure has not been explicitly discussed in the literature,<sup>23</sup> and because of questions arising from the comparison with fixed-nuclei wavefunction calculations, we will review the matrix elements involved.

The effect of an external field is to mix states of opposite parity. For a  $2\Sigma^+$  state, the levels with quantum number  $N$  have the parity  $(-1)^N$ . Second order perturbation terms computed from  $\Delta N = \pm 1$  matrix elements are entirely sufficient to describe the Stark effect for field strengths employed here.

It so happens that for a  $2\Sigma^+$  state, the case  $a$  basis

functions of defined parity (with  $|S_z| = |\Sigma|$ , as well as  $|\Lambda| = 0$  and parity defined) are also the case  $b$  functions. They may therefore be designated by  $N$  in place of parity. The appropriate Hamiltonian eigenfunctions are<sup>24</sup>

$$|JNFm\rangle = 2^{-1/2} \{ |J, \Sigma = \frac{1}{2}, Fm\rangle$$

$$+ (-1)^{J+N+1/2} |J, \Sigma = -\frac{1}{2}, Fm\rangle \}. \quad (6)$$

Stark effect matrix elements have a rigorous selection rule of  $\Delta\Sigma = 0$ , since the electric field does not interact with the electron spin. If the electric field is along the  $z$  axis, the matrix elements are<sup>25</sup>

$$\begin{aligned} \langle JNFm | \mu \cdot \mathbf{E} | J'N'F'm \rangle &= \{ \langle J \frac{1}{2} Fm | \mu \cdot \mathbf{E} | J' \frac{1}{2} F'm \rangle + (-1)^{N+N'+J+J'+1} \langle J, -\frac{1}{2}, Fm | \mu \cdot \mathbf{E} | J', -\frac{1}{2}, F'm \rangle \} / 2 \\ &= E_z (-1)^{J+1+J'+F+F'} C(F1F; m0) [(2J+1)]^{1/2} W(FJF'J'; 11) C(J1J'; \frac{1}{2}0) \mu_{\Sigma} \delta_{N,N'+1}, \end{aligned} \quad (7)$$

where the  $C$  and  $W$  functions are Clebsch-Gordan and Racah coefficients, respectively. The last expression is obtained from the fact that for half-integral  $J$

$$\{ C(J1J'; \frac{1}{2}0) + (-1)^{N+N'+J+J'+1} C(J1J'; -\frac{1}{2}0) \} / 2 = C(J1J'; \frac{1}{2}0) \{ 1 + (-1)^{N+N'+2J} \} / 2 = C(J1J'; \frac{1}{2}0), \quad \text{if } N - N' = \pm 1. \quad (8)$$

The second-order Stark shifts are computed by summing over all  $\Delta N = \pm 1$  interactions. Degenerate perturbation theory applies for the case of off-diagonal elements.<sup>24</sup> Thus, the matrix elements of the second-order Stark effect  $H_S^{(2)}$  within a given  $N$  level are

$$\begin{aligned} \langle JNFm | H_S^{(2)} | J'NF'm \rangle &= \sum_{\bar{J}\bar{F}} \sum_{\bar{N}=\pm 1} \langle JNFm | \mu \cdot \mathbf{E} | \bar{J}\bar{N}\bar{F}m \rangle \langle \bar{J}\bar{N}\bar{F}m | \mu \cdot \mathbf{E} | J'NF'm \rangle \\ &\times \{ [E(JNF) - E(\bar{J}\bar{N}\bar{F})]^{-1} + [E(J'NF') - E(\bar{J}\bar{N}\bar{F})]^{-1} \} / 2. \end{aligned} \quad (9)$$

Because of off-diagonal elements, the displacement of energy levels will not be quadratic with  $E$  except in the very low and high field regions. In the latter case, the interaction with the electric field is larger than the rho-doubling and hyperfine energies; therefore the energy levels will correspond to those of a  $1\Sigma^+$  state, for which the Stark shifts of<sup>13</sup>

$$\Delta E = \frac{\mu^2 E^2}{hB} \left[ \frac{N(N+1) - 3M^2}{2N(N+1)(2N-1)(2N+3)} \right] \quad (10)$$

are added to the internal energies. Figure 5 shows the transition to the high field limit for an  $N=1$  level with hyperfine constants as given in Sec. I and with a dipole moment value presented below. The  $M_N=0$  levels deviate upwards,  $M_N = \pm 1$  downwards. The correspondence indicated by Fig. 5 with the high field limits of the  $1\Sigma^+$  Stark effect supplies a corroboration of the computer program used in this work, as well as a clarification of the shifts that occur. However, the highest value of the electric field actually employed for the transition observed here, indicated by the arrow in Fig. 5, is definitely in the low field region.

To determine which rf transitions may be best observed, the two-level double resonance intensity formula is applied to each appropriate pair of states<sup>26</sup>:

$$\Delta I_{12} = -2[\rho_{11}^0 - \rho_{22}^0] [\Re \mathfrak{M}_{11} - \Re \mathfrak{M}_{22}] \frac{b_{12}^2}{(\Gamma/2\pi)^2 + 4b_{12}^2 + (\nu - \nu_{12})^2}. \quad (11)$$

Elements of the density matrix  $\rho^0$  and measuring operator  $\mathfrak{M}$  for each  $F, J, m$  state are given in Table III of Paper II. The quantities  $b_{12} = (1 | \mu \cdot \mathbf{H}_1 | 2)$  are the magnetic dipole transition elements. They are determined from Table IV of II after rotation of axes to take into account the experimental fact that the rf field and the static electric field are perpendicular. The resultant spectrum at 5 kV/cm is displayed in Fig. 6. It is evident that the

$J = \frac{3}{2}, F = \frac{5}{2}, |m| = \frac{5}{2} \rightarrow J = \frac{1}{2}, F = \frac{3}{2}, |m| = \frac{3}{2}$  transition at about 115 MHz is the most useful; it has the greatest Stark shift, is most free of blending, and has the most intensity. For experimental reasons discussed below, only this transition was used to determine the dipole moment. No search was made for the other Stark-shifted resonances.

## B. Experimental

Measurement of the electric dipole moment by means of the Stark shift requires parallel plate electrodes to produce a uniform constant electric field, oriented so as to permit the existence of an rf magnetic field in the scattering region. The latter requirement essentially precludes parallel orientation of rf magnetic and static electric fields, but presents no difficulties for perpendicular orientation, for which  $\Delta m = \pm 1$  resonances occur. The most intense resonance, given above, is easily observed despite the increased instrumentally scattered light and the restricted view of the scattering region caused by the electrode plates.

The cells used for the Stark effect experiments consisted of a 1 cm slice of  $1\frac{1}{2}$  in. square quartz tubing (Wilma Glass Co.) epoxied between two 0.125 in.  $\times$  2 in.  $\times$  2 in. flat copper plates. A sidearm on one quartz face serves as a gas inlet. The quartz edges were lapped to parallel so that, in the final version, the plates were equidistant to  $\pm 0.02$  mm of a 10.93 mm spacing, as measured by micrometer calipers to  $\pm 0.01$  mm. For parallel plates separated by one-fifth their width, our calculations<sup>27</sup> indicate that the fringing inhomogeneity over the central scattering region of the dimension of one gap width is  $< 0.1\%$ . The major source of error in this design, which could be reduced in an improved version, arises because the quartz walls are about one gap-width from the viewing region. Although the quartz

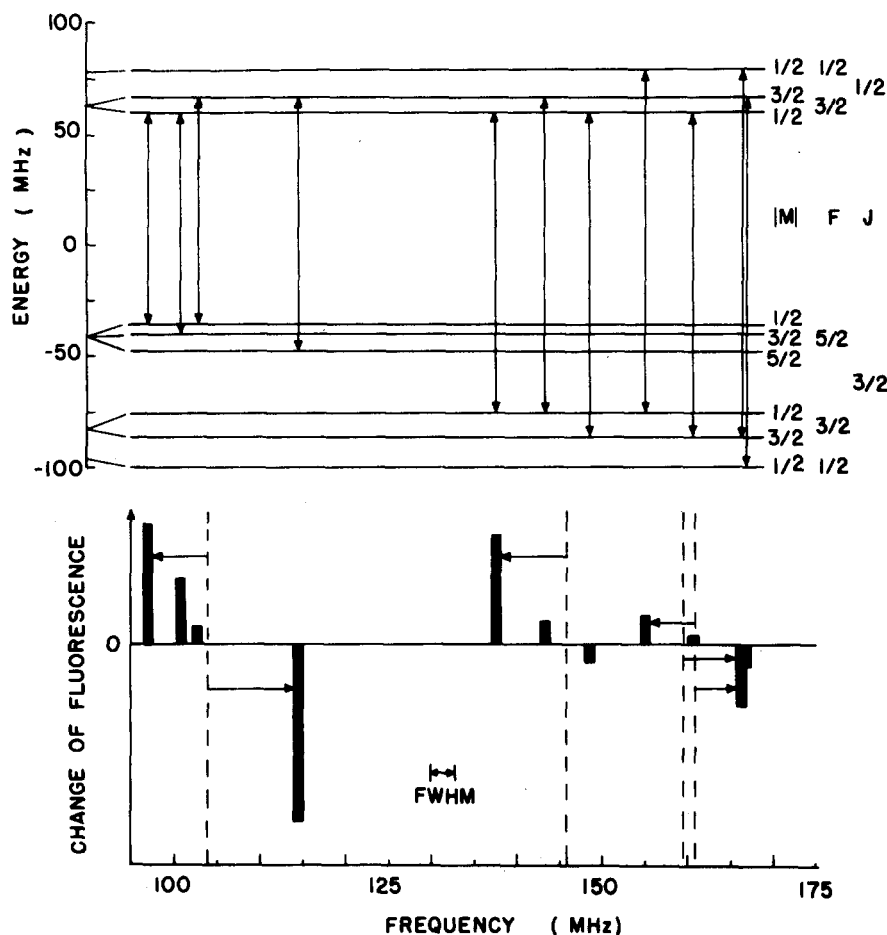


FIG. 6. Computed  $N=1, v=3$ , NO A  $2\Sigma^+$  Stark energy level diagram and corresponding ODR intensities at 5 kV/cm for an rf field of 1 G (rms) perpendicular to the static electric field. In the lower part, the horizontal arrows represent the Stark shifts from the zero-field resonances indicated by vertical dashed lines.

dielectric itself, being parallel to the field, would not produce a distortion, the small bead of epoxy dielectric could easily reduce the field by a percent or so, and hence affect the field in the scattering region by perhaps several tenths of a percent. The power supply (Spellman 10 kV model) was stable to 0.05%, the voltage divider (Fluke 80E) was rated at 0.01% accuracy, and the DVM was given a rating of 0.01% by the manufacturer (Digitec, Inc.). Therefore, the error in the value for the electric field strength is primarily determined by the effects of the epoxy seal, and is taken to be  $\pm 0.5\%$  at the  $1\sigma$  confidence level.

In performing the Stark effect experiments, the fluorescent cell is placed in the rf loop shown as in Fig. 2 with the Stark plates vertical. The fluorescence signal is detected by a phototube mounted below so as to look between the plates. The entrance and exit windows of the cell were masked to minimize the scattering of light by the cell into the photomultiplier. An analyzer in front of the phototube selects light polarized parallel to the electric field. With 25 mtorr NO pressure,  $10^7$  photoelectrons from fluorescent light were detected, as compared with 5 times as many from instrumental scatter, at best. Although the 1961 Å light exceeds or is comparable to the photoelectric work function of many materials, including copper, gaseous discharge breakdown generally occurred only after an hour or so of operation with 7 kV applied across the Stark plates, and was attributed to slow outgassing of the cell.

### C. Stark effect data

The data for the Stark effect consists of four observations of the  $F=\frac{3}{2}, J=\frac{5}{2}, |m|=\frac{5}{2} \rightarrow F=\frac{1}{2}, J=\frac{3}{2}, |m|=\frac{3}{2}$  transition performed with the cell described above. A typical resonance scan (45 min of signal averaging) for the Stark effect is displayed in Fig. 7.

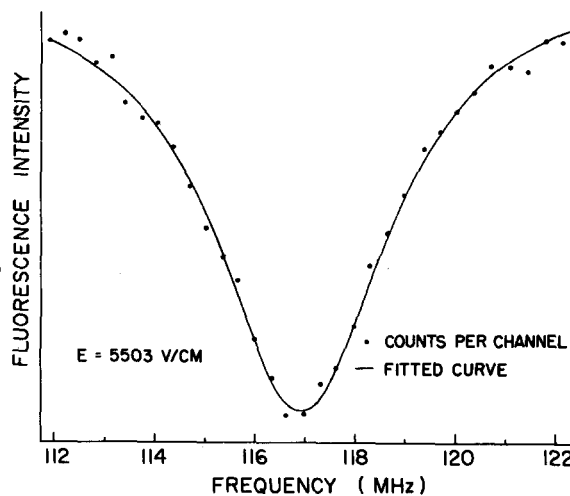


FIG. 7. Typical data for the Stark shifted resonance indicated in Fig. 5. The solid line represents the best fit to a Lorentzian line shape.

In analyzing the Stark effect data, off-resonance interactions (discussed in Paper II) involve a large number of interacting states for the  $\Delta m = \pm 1$  transitions. Because the observed transition has the greatest intensity and is free of blending, the effect of the off-resonance interactions would be expected to produce a displacement of the apparent line center of less than 40 kHz. Line centers were therefore obtained simply by fitting the resonance data to Lorentzian line shapes. The results are quoted in Table III. The uncertainty in the electric field strength given in Table III is relative only and does not include the ambiguous effects of the epoxy seal discussed above.

Because of the surprisingly large value of the dipole moment reported below, it is pertinent to add that approximate measurements of the Stark shift were made with a smaller cell, six months previously to those reported in Table IV. Entirely different means of producing and measuring the electric field were used. The two sets of data agreed to within the 10% experimental error of the earlier measurements.

#### D. Polarizability contribution to the Stark shift

Since Stark effects on the order of 1 MHz at 5 kV/cm have been observed in Rydberg states of alkali atoms,<sup>28</sup> it is evident a small part of the effect observed here will be due to polarization of the outer electron. In accord with the situation in atoms, it may be conjectured that the Rydberg  $3s-3p$  interaction in NO will predominate in the polarizability calculation for the  $A$  state. Oscillator strengths measured from infrared emission intensities by Wray<sup>29</sup> are in accord with this: He obtains  $f = 0.70$  for the (0,0) band of the  $C^2\Pi(3p\pi)-A^2\Sigma^+(3s\sigma)$  transition, and  $f = 0.18$  for the (0,0) band of the  $D^2\Sigma^+(3p\sigma)-A^2\Sigma^+(3s\sigma)$  transition, thereby exhausting almost 90% of the sum rule. If the same values are assumed to apply to the (3,3) bands, these figures may be used to estimate the polarizability contribution to the observed Stark effect.

The relationship between oscillator strength  $f_{ab}$  and transition moment  $\mu_{ab}$  in debyes for the  $a \rightarrow b$  vibronic transition may be obtained from the equation<sup>30</sup>

$$\mu_{ab} = 1.46 \times 10^3 [f_{ab}/g\sigma]^{1/2}, \quad (12)$$

where  $\sigma$  is the wave number of the transition and  $g$  is the degeneracy of the upper state. The pertinent data are given in Table IV. The vibronic matrix elements  $\langle A, v=3 | r | C, v=3 \rangle$  and  $\langle A, v=3 | r | D, v=3 \rangle$  are calculated to be within 0.03 Å of the corresponding values for the

TABLE III. Measurements of the Stark effect for the  $J = \frac{3}{2}$ ,  $F = \frac{3}{2}$ ,  $|m| = \frac{3}{2}$  to  $J = \frac{1}{2}$ ,  $F = \frac{3}{2}$ ,  $|m| = \frac{3}{2}$  transition in  $v=3$ ,  $N=1$  of NO  $A^2\Sigma^+$ .

Run	Electric field (V/cm)	Observed frequency (MHz)	Fitted frequency (MHz)
1	4580 ± 30	112.63 ± 0.2	112.672
2	4580 ± 30	112.38 ± 0.6	112.672
3	5500 ± 40	116.92 ± 0.07	116.919
4	5503 ± 40	116.97 ± 0.1	116.935

TABLE IV. Data on  $3p-3s$  Rydberg-Rydberg transitions in NO.

	$C^2\Pi-A^2\Sigma^+$	$D^2\Sigma^+-A^2\Sigma^+$
	$3p\pi-3s\sigma$	$3p\sigma-3s\sigma$
$\nu_{00}(\text{cm}^{-1})$	8167 <sup>a</sup>	9092 <sup>a</sup>
$f_{00}$	0.70 <sup>b</sup>	0.18 <sup>b</sup>
$\langle 3p   \mu   3s \rangle$	9.56 D	6.50 D

<sup>a</sup>From Ref. 3c.

<sup>b</sup>From Ref. 29.

$\langle A0 | r | D0 \rangle$  elements. Thus, the transition moments are not expected to change appreciably in going from the (0,0) bands to the (3,3) bands. This assumes that mixing of the repulsive  $A^2\Sigma^+$  with the  $D^2\Sigma^+$  state does not affect this conclusion (see below). For the NO Rydberg states, the  $\Delta v = 0$  "selection rule" is nearly exact. Even though the  $D$  state potential departs slightly from that of the other Rydberg states, the  $A-D$  (3,3) vibrational overlap is calculated to be 0.998.

The polarizability formula<sup>13</sup> contains a sum over states:

$$\langle FJN\eta m | H^p | FJN\eta m \rangle = E_z^2 \sum_{\eta' F' J' N' \eta' m'} \frac{|\langle FJN\eta m | \mu | F' J' N' \eta' m \rangle|^2}{E(FJN\eta m) - E(F' J' N' \eta' m)}, \quad (13)$$

where in this case  $\eta$  refers to the  $A^2\Sigma^+$  state, and  $\eta'$  to either  $D^2\Sigma^+$  or  $C^2\Pi$  ( $v=3$  in all cases). Since the internal energy differences are small compared to the electronic energy intervals, the energy denominators may be factored out for each interacting electronic state. For the interaction with  $C^2\Pi$ , the angular part of the sum in the numerator is exactly that which occurs in the  $A^2\Sigma^+-X^2\Pi$  fluorescence measuring operator  $\mathfrak{M}$ , defined in Paper II. Table III of II shows that the difference of this sum for  $z$  polarization between the two levels connected by the observed Stark effect transition is  $0.18 (\mu_{AC} E_z)^2$ . For the  $A-D$  interaction, the difference in the sums between the two terminal levels of the observed Stark effect is  $0.12 (\mu_{AD} E_z)^2$ . In view of the energy intervals given in Table IV, the total polarizability effect from these two interactions is

$$\Delta E^p = 2.14 \times 10^{-2} \text{ MHz}/(\text{kV}/\text{cm})^2. \quad (14)$$

The uncertainty in this correction due to the uncertainty in Wray's transition moments is probably about 25%.

After subtracting the polarizability effect, which amounts to about a 3% correction, the experimental data are combined with the zero-field data in a least square fitting program. The internal standard deviation for the dipole moment from the fit is 0.002 D ( $1\sigma$ ). Thus, the major contribution to the uncertainty in the dipole moment arises from the unknown effect of the epoxy seal on the electric field strength, and to a lesser extent from the polarizability correction and from the neglect of rf-resonance effects on the line shape. The result we obtain for the dipole moment is

$$\mu_A(v=3) = 1.10 \pm 0.03 \text{ D}, \quad (15)$$

where the uncertainty is felt to be comparable to three

standard deviations.

### III. DISCUSSION

#### A. Hyperfine parameters

The value obtained for the unpaired electron-spin density at the  ${}^{14}\text{N}$  nucleus, which is derived from  $b+c/3$ , may be compared with calculations from SCF or CI theory for the lowest  ${}^2\Sigma^+$  state of NO. Table II shows that a configuration interaction calculation by Green<sup>31</sup> does indeed result in very close agreement with the experimental value. The difference between the CI value and the single-configuration result<sup>32</sup> indicates that, by this criterion, the A state does involve some excitation of the core orbitals.

For the  ${}^{14}\text{N}$  nuclear-spin-electron-spin dipolar interaction  $c$  (defined in Sec. I), the agreement with the CI wavefunction is less exact but not far from the limits of experimental error. On the other hand, there is a significant discrepancy for  $eqQ$ , which involves the electric field gradient at the N nucleus from all electrons and the O nucleus rather than simply an unpaired electron interaction. The experimental value for the A state is similar to the experimental<sup>33</sup> and theoretical values<sup>31,32</sup> of  $eqQ_0$  of the X  ${}^2\Pi$  state. While the extraction of this parameter is dependent on the line shape analysis, the sensitivity of this analysis to variations of the rf magnetic field with frequency cannot, to the best of our knowledge, account for more than the quoted uncertainty. It may be that vibronic mixing effects or configuration interaction effects at  $R > r_e$ , discussed in connection with the Stark effect, are involved here also. It may also be that, as has been noted for the lithium atom,<sup>34</sup> calculated values of this parameter do not converge as fast as other quantities as more configurations are included.

#### B. The rho-doubling constant

The phenomenological spin-rotation interaction  $\gamma\mathbf{N} \cdot \mathbf{S}$  for a  ${}^2\Sigma$  state encompasses several effects. In particular,  $\gamma$  represents the "true" magnetic interaction between the magnetic moment of the electron and the magnetic field produced by the rotating nuclei (diagonal  $\mathbf{N} \cdot \mathbf{S}$  interaction) as well as off-diagonal spin-orbit interactions with  ${}^2\Pi$  states. Recently, Knight and Weltner<sup>15</sup> reviewed the data for  ${}^2\Sigma$  states and found that off-diagonal spin-orbit interactions estimated from ESR measurements of the  $g$  tensor agreed remarkably well with the observed  $\gamma$  values. Since our observed rho-doubling constant for the NO A state is an order of magnitude less than for most other  ${}^2\Sigma$  states, it is of interest to examine the relative contributions to the value of  $\gamma$ . Furthermore, the identity of the  ${}^2\Pi$  state or states that contribute to  $\gamma$  is of interest not only to establish spin-orbit intermixing in the  ${}^2\Sigma^+$  wavefunction but also to estimate the possible variation of  $\gamma$  with  $v$  and with  $N$ .

The operator needed to compute the diagonal  $\mathbf{N} \cdot \mathbf{S}$  term is given by Veseth<sup>35</sup> as

$$H_{SR} = \mathbf{N} \cdot \sum_i \eta(i) \mathbf{s}_i + \mathbf{N} \cdot \sum_{i \neq j} \mu(i, j) (\mathbf{s}_i + 2\mathbf{s}_j), \quad (16)$$

where

$$\eta(i) = \frac{e^2 \hbar}{2m^2 c^2 R^2} \sum_k Z_k \left( \frac{1}{|\mathbf{r}_i - \mathbf{R}_k|} - \frac{(\mathbf{r}_i - \mathbf{R}_k) \cdot \mathbf{R}_k}{|\mathbf{r}_i - \mathbf{R}_k|^3} - \frac{r_i^2 - r_{ik}^2}{2|\mathbf{r}_i - \mathbf{R}_k|^3} \right), \quad (17)$$

and

$$\mu(i, j) = \frac{-e^2 \hbar}{4m^2 c^2 R^2} \frac{\mathbf{r}_{ij} \cdot \mathbf{r}_i + r_{ij} r_{ij}}{r_{ij}^3}, \quad (18)$$

where  $Z_k$  and  $\mathbf{R}_k$  denote the charge and center-of-mass coordinate of the  $k$ th nucleus, and  $\mathbf{r}_i$  is the coordinate of the  $i$ th electron measured from the center of mass.

For the NO A state, the evaluation of Eq. (18) reduces to only the  $\eta(i)$  term if we adopt the simple model of a Rydberg 3s electron centered about a unit charge located at the center of charge of the  $\text{NO}^+$  core. Then the summation consists of only one term, with  $Z_k = 1$ , and  $\mathbf{R}_k = 0.14 \text{ \AA}$ , which is the displacement of the center of charge from the center of mass obtained from the calculation of Jungen and Lefebvre-Brion.<sup>36</sup> For this calculation, we use a 3s orbital with a single zeta which reproduces the value of  $1/r$  obtained from the SCF calculation.<sup>32</sup> For such a model, in which the core is approximated as a monopole, the dominant term in (17) is the first term, which represents simply a kinematic effect. There is a "reverse Thomas precession" of the s electron with respect to the rotating nuclear frame. The second term in (17) is zero for a spherically symmetric outer electron, while the third term cancels about one-third of the first term. The resultant diagonal contribution to  $\gamma$  for this model is 3 MHz. However, the effect of the penetration of the s electron into the core is poorly considered in this oversimplified picture.

To continue the multipole expansion, one might arrange a distribution of charges in the rotating frame to reproduce the  $\text{NO}^+$  quadrupole moment, which has been both measured<sup>3b</sup> and calculated.<sup>32,36</sup> (There is no dipole moment about the center of charge.) From rough estimates, it appears possible that such charges might produce a rotational magnetic moment whose interaction with the electron spin is larger in absolute value than the monopole result quoted above. At this point, a simple distribution of point charges becomes a dubious approximation, and *ab initio* wavefunctions are definitely needed. It appears quite unlikely, however, that the interaction (16) would be more than 10% of the rho-doubling value reported in this work.

We are next led to examine off-diagonal spin-orbit contributions to  $\gamma$ . The effective spin-rotation constant arising from  ${}^2\Sigma^+ - {}^2\Pi$  interactions is obtained from Van Vleck<sup>37</sup>:

$$\gamma_{SO} = -2 \sum_{v'} \frac{\langle {}^2\Pi, v' | AL_z | {}^2\Sigma^+, v \rangle \langle {}^2\Pi, v' | BL_z | {}^2\Sigma^+, v \rangle}{E({}^2\Sigma^+, v) - E({}^2\Pi, v')}. \quad (19)$$

In NO, there exist  ${}^2\Pi$  Rydberg states,  ${}^2\Pi$  excited non-Rydberg states (of which B  ${}^2\Pi$  is closest to A  ${}^2\Sigma^+$ ), and the X  ${}^2\Pi$  ground state as possible candidates.

Since Rydberg orbitals have almost exact values for the orbital angular momentum quantum number  $l$ , interactions between the 3s  $\sigma$  A state and Rydberg  $n p \pi$  or  $n d \pi$

states are expected to be small because the  $L_+$  operator will only connect states of equal  $l$ . Accordingly, from SCF wavefunctions, Hall<sup>38</sup> obtains for the  $A-C$  ( $3s\sigma-3p\pi$ ) interaction  $\langle A^2\Sigma^+ | AL_+ | C^2\Pi \rangle < 1 \text{ cm}^{-1}$ . Interaction of the  $A$  state with other Rydberg states is undoubtedly even less.

The three lowest non-Rydberg  $^2\Pi$  states, arising from the configuration  $\cdots (5\sigma)^2 (2\pi)^3 (3\pi)^2$  differ by two molecular orbitals from  $A^2\Sigma^+$ , which has the configuration  $\cdots (5\sigma)^2 (2\pi)^4 3s\sigma$ . Therefore, the matrix element of the one-electron operator  $BL_+$  in (19) vanishes unless configuration interaction is included. However, configuration mixing is always present to some extent, and the  $AL_+$  operator contains two-electron operators. The possible effect of the  $B^2\Pi$  state in particular deserves close attention because its vibrational levels are interspersed between those of the  $A$  state; even a small interaction could mean that  $\gamma$  would have a large variation with  $N$  and  $v$ . Although no  $A-B$  interaction has yet been reported,<sup>38,64</sup> we have reexamined the optical data so as to establish a minimum upper bound for  $\langle A^2\Sigma^+ | AL_+ | B^2\Pi \rangle$ .

The most favorable  $A-B$  perturbation actually occurs in  $v=3$  of the  $A$  state, whose rotational levels intersect  $B^2\Pi(v=6)$  near  $N=18$ . Figure 8 shows energy levels computed from data of Lagerqvist and Miescher<sup>3b</sup> and from Engleman and Rouse.<sup>64</sup> Since there is data on the  $A$  state through the crossing, residuals in the least squares fit to the  $^2\Sigma^+$  Hamiltonian may be examined for evidence of small perturbation shifts. At the top of Fig. 8 we have plotted residuals for the indicated  $J, N$  levels averaged from unblended lines of all observed branches in the (3, 9) and (3, 10) bands.<sup>6e</sup> Data from branches such as  $Q_1$  and  $Q_2$  have been included, since the satellite doublet components are one-third the intensity of the principal line in this region and are spaced nearly a spectral line width apart. The closest degeneracy is clearly that for  $J=17.5, N=18$ . However, the upper component of  $B^2\Pi$ , which lies just  $1.5 \text{ cm}^{-1}$  above the  $A$  state level, is primarily  $^2\Pi_{3/2}$  in character; the coefficient of  $^2\Pi_{1/2}$  in the wavefunction is 0.375. Since only the  $^2\Pi_{1/2}$  part of the wavefunction is connected to  $^2\Sigma^+$  by the  $AL_+$  operator, less exact degeneracies with the lower  $^2\Pi$  components, which have more  $^2\Pi_{1/2}$  character, are almost as sensitive to an  $A-B$  interaction. When all such possibilities are considered with respect to the averaged residuals plotted in Fig. 8, we conclude that  $\langle B^2\Pi, v=6 | AL_+ | A^2\Sigma^+, v=3 \rangle = 0.0 \pm 0.3 \text{ cm}^{-1}$ . From this, one may obtain an upper bound on the contribution of  $B^2\Pi(v=6)$  to the observed  $\gamma$  if one assumes that  $\langle BL_+ \rangle / \langle AL_+ \rangle < \langle B\pi \rangle / \langle A\pi \rangle \cong 1/30$ . Thus from (19) and the above, the contribution of the  $B^2\Pi$  interaction to  $\gamma(v=3)$  for the  $N=1$  level is  $< 0.3 \text{ MHz}$ . However, in using the value of  $\gamma$  found for this level to predict rf rho-doubling frequencies for higher  $N$  levels, attention must be given to the existence of a centrifugal distortion correction to  $\gamma$ , as well as to the fact that only an upper bound has been established for the  $A-B$  (3, 6) interaction.

We next estimate a minimum upper bound on the total contribution of all  $B^2\Pi(v)$  levels to  $\gamma$ . Since the  $A-B$  (3, 6) vibrational overlap is computed to be 0.075, we obtain from the above bound  $\langle A^2\Sigma^+ | AL_+ | B^2\Pi \rangle = 0 \pm 4$

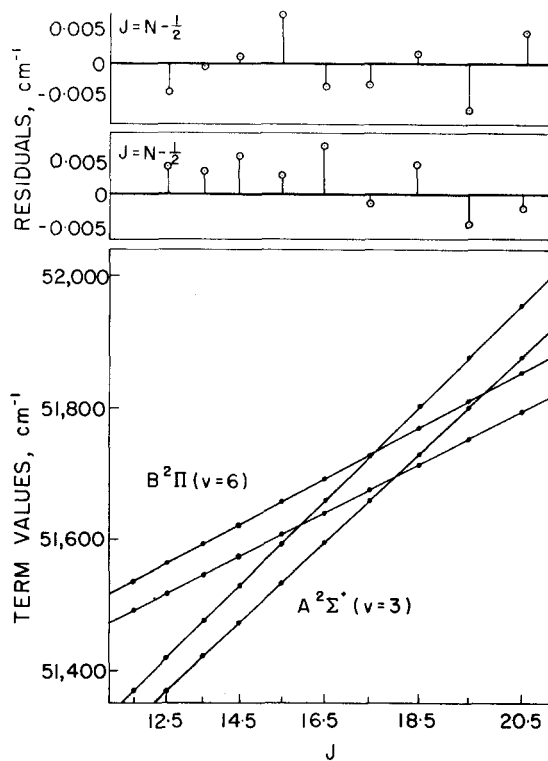


FIG. 8. Investigation of possible perturbation between the NO  $A^2\Sigma^+(v=3)$  and  $B^2\Pi(v=6)$  states. Term values are plotted in the lower portion; the residuals from least squares fits to the  $A-X$  (3, 9) and (3, 10) bands are given in the upper portion for each of the rho-doublet components.

$\text{cm}^{-1}$ . This null result is consistent with the observation of Jungen and Miescher<sup>3e</sup> that no mechanism operates to produce  $ns\sigma^2\Sigma^+-B^2\Pi$  perturbations, in distinction to  $np\sigma^2\Sigma^+-B^2\Pi$  interactions obtained by configuration interaction with  $np^2\Pi$  Rydberg states.

Assuming again that  $\langle BL_+ \rangle / \langle AL_+ \rangle < 1/30$ , and applying the approximation

$$\gamma_{SO} \cong -2 \langle ^2\Pi | AL_+ | ^2\Sigma^+ \rangle \langle ^2\Pi | L_+ | ^2\Sigma^+ \rangle \times \sum_{v'} \frac{\langle ^2\Sigma^+ v | ^2\Pi v' \rangle \langle ^2\Pi v' | B(R) | ^2\Sigma^+ v \rangle}{E(^2\Sigma^+ v) - E(^2\Pi v')} \quad (20)$$

to (19), we conclude that the total contribution of the  $B$  state to  $\gamma(v=3)$  is  $< 3 \text{ MHz}$ . This estimate implies that the variation of  $\gamma$  with  $v$  will be very small because close-lying  $^2\Pi$  states do not contribute substantially.

By the preceding process of elimination, we look to the  $X^2\Pi$  state as the source of the primary contribution to  $\gamma$ . Since the  $X$  state is a valence state with configuration  $\cdots (5\sigma)^2 (2\pi)^4 3\pi$ , which differs by only one orbital from the  $A$  state, it is not surprising that it might provide the predominant coupling of the Rydberg electron with the nuclear frame. Recently, Lefebvre-Brion<sup>39</sup> has computed the pertinent electronic matrix elements from improved SCF wavefunctions. She obtains

$$\begin{aligned} \langle X^2\Pi | AL_+ | A^2\Sigma^+ \rangle &= 20 \text{ cm}^{-1} \\ \langle X^2\Pi | L_+ | A^2\Sigma^+ \rangle &= 0.47. \end{aligned} \quad (21)$$

If the  $A-X$  interaction were in fact to account for *all* of the observed  $\gamma$ , then from the sum in Eq. (20) we obtain

$$\langle X^2\Pi | AL_+ | A^2\Sigma^+ \rangle \langle X^2\Pi | L_+ | A^2\Sigma^+ \rangle \cong 29 \text{ cm}^{-1}. \quad (22)$$

The difference between this and the product of the theoretical quantities,  $9.4 \text{ cm}^{-1}$ , may be attributed to the terms discussed previously, to variations of these matrix elements with internuclear distance, and to approximations in the wavefunctions and in the form of the spin-orbit operator used. Consequently, we conclude that the observed value of  $\gamma$  is substantially explained by off-diagonal spin-orbit interaction with the  $X^2\Pi$  state.

Neither the  $A-X$  interaction nor the diagonal  $N \cdot S$  term will introduce a significant variation of  $\gamma$  with  $v$ . This conclusion is consistent with negative results of a search for the rho-doubling transition in  $N=10$ ,  $v=1$ , using the Te 2147 Å atomic line<sup>10</sup> as the optical pumping source. This search employed a transmission line oscillator<sup>40</sup> rather different in concept from the apparatus described above, and more suited to scans in the 400–800 MHz region. Conditions were more than ample for observation of the rho-doubling resonance signal for values of  $|\gamma| < 74 \text{ MHz}$ , yet none was observed. Technical difficulties prevented a search at higher frequencies corresponding more closely to the expected value of  $\gamma$  ( $v=1$ )  $\cong \gamma$  ( $v=3$ ).

The reported value of the spin-rotation constant is far more precise than any previous determination of  $\gamma$  from the optical spectrum. However, in conjunction with the computation of the residuals presented in Fig. 8, we have extracted an improved value for  $\gamma$  ( $v=3$ ) from the data of Engleman *et al.*<sup>6e</sup> In order to do this, it was necessary to fix the  $J$  dependence of the  $^2\Pi$  spin-orbit parameter,  $A_D$ , equal to zero, since  $A_D$  is highly correlated with  $\gamma$  in a simultaneous least squares fit to the upper and lower state energy levels.<sup>24</sup> When the optical data are used in this manner, the uncertainty in the fitted value of  $\gamma$  is substantially reduced from the published results of Ref. 6d. Upon averaging the values from the (3,9) and (3,10) bands, we obtain  $\gamma$  ( $v=3$ ) =  $-90 \pm 15 \text{ MHz}$  ( $3\sigma$ ), which is consistent with the ODR determination.

By using the known value of  $\gamma$  as a fixed parameter in the least squares fitting procedure, it is possible to break the correlation between  $\gamma$  and  $A_D$ . In this manner, we obtain for the  $X^2\Pi$  state,  $A_D$  ( $v=9$ ) =  $-9.8 \pm 5.0 \times 10^{-5} \text{ cm}^{-1}$ , and  $A_D$  ( $v=10$ ) =  $-4.4 \pm 4.3 \times 10^{-5} \text{ cm}^{-1}$ . Previously, James<sup>41</sup> has searched for values of this parameter in the infrared spectral data for NO, but found it too small for a reliable determination. The sign and order of magnitude of the above values agree with the approximation  $A_D = [2(A_{v+1} - A_v)D_{v=0}] / [\alpha_e + 6B_e^2/\omega_e]$  given by Veseth.<sup>42</sup>

A reanalysis of the optical data for  $A-X$  ( $1, v''$ ) bands was also performed to obtain information on the variation of  $\gamma$  with  $v$ . With  $A_D$  set equal to zero as above, least squares fits to the data of Ref. 6e for the (1,0), (1,6), and (1,7) bands gave  $\gamma$  ( $v=1$ ) =  $-92 \pm 58$ ,  $-37 \pm 36$ , and  $-86 \pm 42 \text{ MHz}$ , respectively. ( $3\sigma$  is given, as in all data quoted in this paper.) Despite its smaller uncertainty, the value obtained from the (1,6) band is questionable because it includes only a few transitions with

$J' > 20$ . (States of higher  $J'$  are most sensitive to the value of  $\gamma$ .) Therefore, we conclude that the optical data does suggest that  $\gamma$  varies only slightly with  $v$ .

### C. The electric dipole moment

The measured value of the dipole moment is certainly the most intriguing of the results obtained from these experiments. If there is not an undetected error in the experimental procedure or in the analysis of the Stark effect, there exists a substantial discrepancy between the experimental result and the convergent fixed-nuclei calculation performed for  $R=r_e$ . While possible contributing factors may be identified, no explanation can be verified at present.

Either from a rudimentary picture of a Rydberg state or from published calculations, one concludes that the dipole moment should be much smaller than our measurements indicate. If the  $A^2\Sigma^+$  state is described by a spherically symmetric Rydberg electron centered about the center of charge of the  $\text{NO}^+$  core, then the dipole moment would be zero. Since the SCF calculation of Green<sup>32</sup> gives  $\langle r \rangle = 3.1 \text{ Å}$  for the  $3s\sigma$  outer electron as compared with  $r_e = 1.06 \text{ Å}$ , the electron will penetrate the core to only a small extent, and therefore the Rydberg-core interaction would produce only a rather small departure from the null moment. This expectation is corroborated by exhaustive configuration interaction calculations for the  $A$  state at the equilibrium internuclear distance by Green.<sup>31</sup> The theoretical dipole moment converges to a value of  $0.47 \pm 0.03 \text{ D}$  ( $\text{N}^+\text{O}^-$ ) for  $R=1.06 \text{ Å}$ . On the basis of a procedure that has been found to be valid for valence states, Green has estimated the effect of vibrational averaging from the variation of the dipole moment computed from SCF wavefunctions at other  $R$  values. He obtains by this means  $\mu = 0.40 \pm 0.10 \text{ D}$  for  $v=3$ . The discrepancy with the experimental value reported above,  $1.10 \pm 0.03 \text{ D}$ , is surprisingly large. Until now, theoretical calculations and experimental dipole moment determinations have usually been brought to agreement within 0.1 D or so. (For a list of such comparisons, see the review article by Green.<sup>43</sup>)

In view of the apparent discrepancy, it might be conjectured that either the Stark effect transition has been misassigned, the electric field is incorrectly calibrated, or that there is a numerical error in the analysis. Note, however, the agreement of the experimentally-determined hyperfine structure parameters with other results of the same *ab initio* calculation and the agreement of  $\gamma$  with the optical data provide a confirmation of the quantum number assignment of the zero-field resonances. Moreover, because only the  $J = \frac{3}{2}$ ,  $F = \frac{5}{2}$ ,  $|m| = \frac{3}{2} \rightarrow J = \frac{1}{2}$ ,  $F = \frac{3}{2}$ ,  $|m| = \frac{3}{2}$  transition moves to higher frequency with increasing electric field as observed, the assignment of the Stark effect resonance is unambiguous. It is also pertinent to note again that measurements of the Stark shift were obtained six months apart using different apparatus to produce and measure the electric field; these independent measurements agreed to within their combined experimental uncertainty of 10%. Finally, the computer fitting program, which agrees with the  $^2\Sigma^+$  high field limit as noted above, is

the same program<sup>44</sup> used by Weinstock and Zare<sup>9</sup> to deduce the dipole moment for the  $A^2\Sigma^+$  state of OD from level-crossover data. While the OD result differed by 15% from an optical determination and by 6% from a CI calculation, a factor of 2 discrepancy in the fitting program appears out of the question. It would be desirable to have data on the other, less accessible Stark effect transitions indicated in Fig. 6. However, we are unable to identify a source of error in the experimental data or the analysis to account for the discrepancy between the experimental result and fixed-nuclei *ab initio* calculations.

There have been no previous dipole moment measurements for molecular Rydberg states. If the discrepancy in  $\mu$  is indeed real, we may look for explanation in circumstances that apply in this instance which are normally not significant for valence states. Two such possibilities appear upon examination of the  $^2\Sigma^+$  manifold in NO.

As with molecular Rydberg states in general, there exists here a nearby electronic state connected to the  $A$  state by a large  $\Delta l=1$  hydrogenic transition moment, as indicated in Table IV. A small  $s$ - $p$  mixing could result in an appreciable effect on the dipole moment of the  $A$  state. This may be called "dipole borrowing" in analogy to intensity borrowing. Although the configuration interaction calculations have included all such possibilities at  $R=r_e$ , the likelihood for  $3s\sigma$ - $3p\sigma$  intermixing would appear to be increased as one moves from 1.06–1.20 Å because of the convergence of several  $^2\Sigma^+$  potential curves. A recent study by Ben-Aryeh<sup>45</sup> concludes that the shifts of the  $3p\sigma$  D state level from normal Rydberg behavior are consistent with an interaction with the  $A'^2\Sigma^+$  ( $5\sigma$ )<sup>2</sup>( $2\pi$ )<sup>4</sup>  $6\sigma$  repulsive state, as previously suggested.<sup>33</sup> Ben-Aryeh derives a parameter for a limited region of the  $A'$  state potential curve. These results suggest that the  $A'$  state lies 9 eV above the  $A$  state at 1.06 Å, but only 2 eV above the  $A$  state at 1.20 Å. There is also available some partial data on the  $I^2\Sigma^+$  state,<sup>45</sup> a non-Rydberg quasibound state that is assigned the configuration ( $5\sigma$ )<sup>2</sup>( $1\pi$ )<sup>3</sup>( $2\pi$ )<sup>2</sup>. By comparison with isoconfigurational states, the  $I$  state potential curve may be expected to fall from approximately 7 eV above the  $A$  state at 1.06 Å to about 2.5 eV above the outer turning point of  $A$  ( $v=3$ ) at 1.20 Å. In the absence of computational results to the contrary, it therefore appears possible that the effect of configurational mixing could be rather different at 1.20 Å than at  $R=r_e$ . In this case, the variation of  $\mu$  with  $R$  and hence the vibrational averaging would differ from the estimate derived from SCF calculations of the dipole derivative.

The close proximity of several  $^2\Sigma^+$  states noted above also may lead to  $s$ - $p$  mixing through nonadiabatic coupling. Although direct coupling between the  $3s\sigma$ - $3p\sigma$  configurations by nuclear motion appears to be quite small, it is possible to conjecture that here, too, the  $I$  or  $A'$  states may act as intermediaries. We briefly present some of the matrix elements involved to suggest further lines of inquiry on this question.

The leading term neglected in the Born-Oppenheimer approximation is the nuclear kinetic energy operator.

As shown by Van Vleck,<sup>46</sup> elements of the form

$$V_1 = -\frac{\hbar^2}{M} \langle \eta v | \frac{\partial}{\partial R} | \eta' v' \rangle \langle \eta | \frac{\partial}{\partial R} | \eta' \rangle \quad (23)$$

are larger by  $(\hbar\omega_e/B_e)^{1/2}$  than higher order terms. Here  $M$  is the reduced mass,  $|\eta v\rangle$  is the vibrational wavefunction for level  $v$  of the electronic state  $\eta$ , and  $|\eta\rangle$  is the electronic wavefunction, which depends parametrically on the internuclear distance. Terms of the form  $V_1$  will only couple states of the same symmetry. The dependence of the  $F, J, M$  quantum numbers will be unaffected and hence one may deal directly with the reduced dipole matrix elements. Intermixing of a state  $|\eta v\rangle$  by  $V_1$  will produce first-order perturbation corrections to the  $A$  ( $v=3$ ) dipole moment as follows:

$$\begin{aligned} \mu &= {}_1\langle A3 | \mu | A3 \rangle_1 \\ &= \langle A3 | \mu | A3 \rangle + 2 \sum_{\eta, v} \langle \eta v | \mu | A3 \rangle \frac{\langle \eta v | V_1 | A3 \rangle}{E(A3) - E(\eta v)}. \end{aligned} \quad (24)$$

The null result for direct  $3s\sigma$ - $3p\sigma$  Rydberg-Rydberg coupling arises from the contradictory selection rules for the two vibronic factors in the sum. In the harmonic oscillator approximation,  $\langle \eta v' | \mu | A(v=3) \rangle$  requires  $\Delta v = 0$ , while the factor  $\langle \eta v' | V_1 | A(v=3) \rangle$  is nonzero only for  $\Delta v = \pm 1$ . Although the empirical RKR potentials for the  $A$  and  $D$  states depart from harmonic oscillator form and also slightly from each other, we find by explicit calculation of the above elements that the total effect on the dipole moment from Eq. (24) is  $<10^{-4}$  D despite the 6.5 D  $A$ - $D$  transition moment indicated in Table IV. However, the  $v=v'=3$  contribution itself is 0.03 D. (To obtain this, we have used the value of the electronic matrix element  $\langle A | \partial/\partial R | D \rangle = 0.5 \text{ \AA}^{-1}$  obtained by Liu.<sup>47</sup> The resultant value of  $V_1$  for the  $A$ - $D$  (5, 1) interaction is  $0.4 \text{ cm}^{-1}$ , as compared with  $0.28 \text{ cm}^{-1}$  observed spectroscopically by Miescher.)<sup>37</sup> It seems, therefore, that if nonadiabatic effects are to be significant, they must involve more than simply the  $A$  and  $D$  states. The  $305 \text{ cm}^{-1}$  shift of the  $v=3$  level of the  $D$  state implies, by Ben-Aryeh's analysis, that the intermixing of the  $A'$  state is appreciable, with a total coefficient of perhaps 0.15. Clearly, the harmonic oscillator selection rules do not apply to the nonadiabatic coupling between the  $A$  and  $A'$  wavefunctions. It seems possible to conjecture, therefore, that  $A'$  admixture in the  $D$  state wavefunctions may produce an effect on the dipole moment from the  $\Delta v=0$   $A$ - $D$  coupling to a greater extent than 0.03 D, and also may nullify the cancellation effect from the sum over the  $D$  state vibronic levels. To calculate such an effect, one would need in addition to potential curves appropriate off-diagonal elements between the relevant  $^2\Sigma^+$  states:  $A, D, I$ , and  $A'$ .

Both configuration interaction variation with  $R$  and nonadiabatic coupling will produce a variation of the observed dipole moment with  $v$ . As there do not appear to be other coincidences between strong atomic lines and NO absorption lines which pump low  $N$  levels, the technique reported here cannot be used for  $v \neq 3$ . The development of tunable laser sources below 2300 Å or the use of two-photon absorption techniques<sup>48</sup> will make possible a more systematic study of effects that seem to be

suggested by the dipole moment measurement reported here.

## ACKNOWLEDGMENTS

Many people have contributed generously of their time to make this work possible. The experimental work was conducted in the Columbia Radiation Laboratory, and the assistance of the staff is deeply appreciated. We are indebted to L. A. Melton for communicating his discovery of the Se line coincidence prior to publication, to E. M. Weinstock for use of his Se electrodeless lamp, and to W. Nagourney for adapting his signal averaging program to our scanning oscillator. The assistance of R. Coupepez in the design and construction of various rf oscillators was invaluable, as was the delicate quartz glassblowing of J. Gorham.

We warmly thank Ch. Jungen for critical comments on vibronic coupling, R. Engleman for supplying us with his line position data deck, D. L. Albritton for results of his analysis of the NO A and B states, H. Lefebvre-Brion, J. A. Hall, and T. E. H. Walker for calculations of spin-orbit matrix elements, and S. Green and B. Liu for undertaking many *ab initio* calculations pertaining to this work. This work was supported by the National Science Foundation under grant NSF-GP-31336x and by the Columbia Radiation Laboratory through the Joint Services Electronics Program under contract DAA-B07-69-C-0383.

\*Present address.

<sup>1</sup>R. S. Mulliken, *J. Am. Chem. Soc.* **86**, 3183 (1964); **91**, 4615 (1969).

<sup>2</sup>For calculations on diatomic Rydberg states for CO, see H. Lefebvre-Brion and C. M. Moser, *J. Mol. Spectrosc.* **13**, 418 (1964); for NO and BF, see H. Lefebvre-Brion, C. M. Moser, and R. K. Nesbet, *J. Mol. Spectrosc.* **15**, 211 (1965); for N<sub>2</sub>, see H. Lefebvre-Brion and C. M. Moser, *J. Chem. Phys.* **43**, 1394 (1965); for BH and AlH, see F. Grimaldi, A. Le Court, H. Lefebvre-Brion, and C. M. Moser, *J. Mol. Spectrosc.* **20**, 341 (1966); for BH see P. K. Pearson, C. F. Bender, and H. F. Schaeffer III, *J. Chem. Phys.* **55**, 5235 (1971). For the use of model potentials see A. Hazi and S. A. Rice, *J. Chem. Phys.* **48**, 495 (1968) and T. Betts and V. McKay, *J. Chem. Phys.* **54**, 113 (1971).

<sup>3</sup>(a) R. F. Barrow and E. Miescher, *Proc. Phys. Soc. Lond. A* **70**, 219 (1957); (b) A. Lagerqvist and E. Miescher, *Helv. Phys. Acta* **31**, 221 (1958); (c) M. Huber, *Helv. Phys. Acta* **37**, 329 (1964); (d) K. Dressler and E. Miescher, *Astrophys. J.* **141**, 1266 (1965); (e) E. Miescher, *J. Mol. Spectrosc.* **20**, 130 (1966); (f) A. Lagerqvist and E. Miescher, *Can. J. Phys.* **44**, 1525 (1966); (g) Ch. Jungen and E. Miescher, *Can. J. Phys.* **46**, 987 (1968), and (h) **47**, 1769 (1969); (i) Ch. Jungen, *J. Chem. Phys.* **53**, 4168 (1970); (j) E. Miescher, *Can. J. Phys.* **49**, 2350 (1971).

<sup>4</sup>See (a) P. R. Brooks, W. Lichten, and R. Reno, *Phys. Rev. A* **4**, 2217 (1971); (b) R. Jost, M. A. Marechal, and M. Lombardi, *Phys. Rev. A* **5**, 740 (1972); (c) R. S. Freund and T. A. Miller, *J. Chem. Phys.* **59**, 4073 (1973); T. A. Miller and R. S. Freund, *ibid.*, **59**, 4093 (1973) and references contained therein.

<sup>5</sup>A preliminary report of this work appeared in T. H. Bergeman and R. N. Zare, *Bull. Am. Phys. Soc.* **17**, 149 (1972).

<sup>6</sup>(a) R. Schmid, *Z. Phys.* **49**, 428 (1928); (b) L. Gerö and R. Schmid, *Proc. Phys. Soc. Lond.* **60**, 533 (1948); (c) I. Deézi, *Acta Phys. Acad. Sci. Hung.* **9**, 125 (1958); (d) R.

Engleman and P. E. Rouse, *J. Mol. Spectrosc.* **37**, 240 (1971); (e) R. Engleman, P. E. Rouse, H. M. Peek, and V. D. Baiamonte, "The Beta and Gamma Band Systems of Nitric Oxide," Los Alamos Scientific Laboratory Report LA-4364, 1970.

<sup>7</sup>R. S. Berry and S. E. Nielsen, *Phys. Rev. A* **1**, 383 (1970), **1**, 395 (1970); S. E. Nielsen and R. S. Berry, *Phys. Rev. A* **4**, 865 (1971).

<sup>8</sup>P. Felenbok and H. Lefebvre-Brion, *Can. J. Phys.* **44**, 1677 (1966).

<sup>9</sup>For an example of laser saturation spectroscopy, see M. D. Levenson and A. L. Schawlow, *Phys. Rev.* **6**, 10 (1972); for excited state magnetic resonance see Ref. 4c and the review article, D. H. Levy, *Adv. Magn. Reson.* **6** (to be published); for level crossovers, see E. M. Weinstock and R. N. Zare, *J. Chem. Phys.* **58**, 4319 (1973); for double resonance, see R. W. Field and T. H. Bergeman, *J. Chem. Phys.* **54**, 2936 (1971). See also *Méthodes de Spectroscopie Sans Largeur Doppler de Niveaux Excités de Systèmes Moléculaires Simples* (CNRS No. 217, Paris France, 1974).

<sup>10</sup>L. A. Melton and W. Klemperer, *J. Chem. Phys.* **59**, 1099 (1973).

<sup>11</sup>G. zu Putlitz, *Ergeb. Exakten Naturwiss.* **37**, 105 (1965).

<sup>12</sup>T. Bergeman, *J. Chem. Phys.* **61**, xxx (1974).

<sup>13</sup>C. H. Townes and A. L. Schawlow, *Microwave Spectroscopy* (McGraw-Hill, New York, 1955).

<sup>14</sup>(a) R. A. Frosch and H. M. Foley, *Phys. Rev.* **88**, 1337 (1952); (b) H. E. Radford, *Phys. Rev. A* **136**, 1571 (1964).

<sup>15</sup>L. B. Knight, Jr. and W. Weltner, Jr., *J. Chem. Phys.* **53**, 4111 (1970).

<sup>16</sup>K. R. German, T. H. Bergeman, E. M. Weinstock, and R. N. Zare, *J. Chem. Phys.* **58**, 4304 (1973).

<sup>17</sup>This circuit was adapted from one given in the thesis of H. Berg (Harvard, 1964) based on a design of H. G. Robinson.

<sup>18</sup>R. W. P. King, *Transmission Line Theory* (Dover, New York, 1965).

<sup>19</sup>The fitting procedure actually also employed the Stark data (Table III).

<sup>20</sup>E. M. Weinstock, R. N. Zare, and L. A. Melton, *J. Chem. Phys.* **56**, 3456 (1972). See also K. R. German, R. N. Zare, and D. R. Crosley, *J. Chem. Phys.* **54**, 4039 (1971).

<sup>21</sup>H. Bubert, *J. Chem. Phys.* **56**, 1113 (1972).

<sup>22</sup>See, for example, A. Pery-Thorne and F. P. Banfield, *J. Phys. B* **3**, 1011 (1970); and A. J. D. Farmer, V. Hasson, and R. W. Nicholls, *J. Quant. Spectrosc. Radiat. Transfer* **12**, 627 (1972).

<sup>23</sup>The Stark effect for a  $2\Sigma^+$  state without hyperfine structure has been discussed by R. Thomson and F. W. Dalby, *Can. J. Phys.* **46**, 2815 (1968).

<sup>24</sup>See Appendix A of R. N. Zare, A. L. Schmeltekopf, W. J. Harrop, and D. L. Albritton, *J. Mol. Spectrosc.* **46**, 37 (1973).

<sup>25</sup>K. Freed, *J. Chem. Phys.* **45**, 4214 (1966); and A. Carrington, D. H. Levy, T. A. Miller, *Adv. Chem. Phys.* **18**, 149 (1970).

<sup>26</sup>S. J. Silvers, T. H. Bergeman, W. A. Klemperer, *J. Chem. Phys.* **52**, 4385 (1970); R. W. Field and T. Bergeman, *J. Chem. Phys.* **54**, 2936 (1971); Ref. 16.

<sup>27</sup>See also E. Weber, *Electromagnetic Theory* (Dover, New York, 1965), p. 336.

<sup>28</sup>See, for example, R. W. Schneider, A. Lurio, W. Happer, *Phys. Rev. A* **3**, 1209 (1971); and A. Khadjavi, A. Lurio, and W. Happer, *Phys. Rev.* **167**, 128 (1968).

<sup>29</sup>K. L. Wray, *J. Quant. Spectrosc. Radiat. Transfer* **9**, 255 (1969).

<sup>30</sup>This expression may be obtained from formulas in G. Herzberg, *Spectra of Diatomic Molecules* (Van Nostrand, Princeton, New Jersey, 1950), 2nd ed.

<sup>31</sup>S. Green, *Chem. Phys. Lett.* **23**, 115 (1973).

<sup>32</sup>S. Green, *Chem. Phys. Lett.* **13**, 552 (1972).

<sup>33</sup>R. M. Neumann, *Astrophys. J.* **161**, 779 (1970); W. L.

- Meerts and A. Dymanus, *J. Mol. Spectrosc.* **44**, 320 (1972).
- <sup>34</sup>S. Hameed and H. M. Foley, *Phys. Rev.* **6**, 1399 (1972).
- <sup>35</sup>L. Veseth, *J. Phys. B* **4**, 20 (1971).
- <sup>36</sup>C. Jungen and H. Lefebvre-Brion, *J. Mol. Spectrosc.* **33**, 520 (1970).
- <sup>37</sup>J. H. Van Vleck, *Phys. Rev.* **33**, 467 (1929).
- <sup>38</sup>J. A. Hall (private communication).
- <sup>39</sup>H. Lefebvre-Brion (private communication).
- <sup>40</sup>The transmission line oscillator design was suggested to us by Mr. R. Coupepez. See also Ref. 16, Chap. VI.
- <sup>41</sup>T. C. James, *J. Chem. Phys.* **41**, 631 (1964).
- <sup>42</sup>L. Veseth, *J. Phys. B* **3**, 1677 (1970). See also L. Veseth, *J. Mol. Spectrosc.* **38**, 228 (1971), where it is pointed out that  $A_D=2A_J$  cannot be separated from the spin-rotation constant of the  $2\Pi$  state.
- <sup>43</sup>S. Green, *Adv. Chem. Phys.* **25**, 173 (1974).
- <sup>44</sup>The formalism of W. Wentworth, *J. Chem. Educ.* **42**, 96 (1965) was programmed for the  $2\Sigma$  state parameters.
- <sup>45</sup>Y. Ben-Aryeh, *J. Quant. Spectrosc. Radiat. Transfer* **13**, 1441 (1973).
- <sup>46</sup>J. H. Van Vleck, *J. Chem. Phys.* **4**, 327 (1936).
- <sup>47</sup>B. Liu (private communication).
- <sup>48</sup>R. G. Bray, R. M. Hochstrasser, and J. E. Wessel, *Chem. Phys. Lett.* **27**, 167 (1974).